Received 15 March 2023; revised 14 April 2023; accepted 28 April 2023. Date of publication 5 May 2023; date of current version 24 May 2023.

Digital Object Identifier 10.1109/OJAP.2023.3273488

3-D Printed All-Dielectric GRIN Lens Antenna With an Integrated Feeder

ANASTASIOS PARASKEVOPOULOS[1], FRANCESCA MAGGIORELLI[1], ILIR GASHI[1] (Graduate Student Member, IEEE), CRISTIAN DELLA GIOVAMPAOLA[2], MATTEO ALBANI[1] (Fellow, IEEE), AND STEFANO MACI[1] (Fellow, IEEE)

[1]Department of Information Engineering and Mathematics, University of Siena, 53100 Siena, Italy

[2]Wave Up s.r.l., 53100 Siena, Italy

CORRESPONDING AUTHOR: A. PARASKEVOPOULOS (e-mail: paraskevopoulos@diism.unisi.it)

This work was supported by Huawei Technologies Company Ltd., within the joint Innovation Antenna Lab between Huawei and the Department of Information Engineering and Mathematics, University of Siena.

ABSTRACT In this paper we present the design, fabrication, and experimental verification of a new type of Graded-index (GRIN) lens antenna with an integrated feeder. The continuously varying refractive index distribution is chosen appropriately to offer the rays collimation at the lens aperture. It is practically implemented by varying the material density in a host medium, thus realizing a new type of all-dielectric high gain antenna, entirely using 3D printing. This solution can find application to high gain wireless communication and measurement systems. This GRIN lens antenna is printed in one monolithic process and does not require the feeder to be placed at a focal distance, thus complying with more strict space requirements. It accepts interchangeable feeds that can cover a wide frequency range. The directivity and gain are evaluated using near-field measurements in the Ku-band. A 40% measured aperture efficiency is achieved at 14GHz. The challenges and performance limitations that come with 3D printing, as compared to the design of idealized continuous distribution GRIN lenses are discussed.

INDEX TERMS 3D printed antennas, dielectric lenses, inhomogeneous lenses.

I. INTRODUCTION

THE ADVENT of 3D printing in combination with the availability of high dielectric permittivity composite filaments in the market [2] has enabled the fast prototyping of new metamaterial structures. This gives rise to a new sector of dielectric metamaterials and metasurfaces, in which the amplitude and phase of the EM wave propagating through the structure can be manipulated by realizing subwavelength patterning, following a specific permittivity distribution.

During the last decade, numerous studies have appeared in the literature that have qualified 3D printing as a promising technology for realizing complex 3D metamaterial structures. Starting from the characterization of the permittivity and losses for various fused filament materials [3], [4] to the realization of 3D printed structures for new antenna concepts [5], [6], [7], [8], [9], [10], [11], [12], [13], [14], [15]. These structures range from dielectric domes [5], Modulated Dielectric Metasurfaces [6], CP polarizers [7], reflectarrays [8], [9], Risley prisms for 2D beam steering [10] and flat cylindrical [11], [12], [13], [14] and 3D GRIN lenses [15]. The principle of operation of the proposed GRIN lenses [11], [12], [13], [14] is to transform a spherical wave into a plane wave to produce highly directive beams. Resorting to the Geometrical Optics (GO) approximation, having a plane wave at the lens output correspond to parallel rays at the lens output, namely to collimated ray-paths. This result can be obtained through the variation of the lens permittivity and possibly of the shape [15], [16]. Thus, GRIN lenses can focus the EM energy towards a specific direction of interest.

However, in all the aforementioned GRIN lens studies, the lens feeder has to be placed at a focal distance from the lens surface and requires additional mounting and alignment efforts resulting to a cumbersome system. Only recently in [17], a shortened joint 3D printed GRIN lens together with metalized 3D printed horn antenna was realized offering a more compact counterpart to traditional standard gain horn

antennas. Despite the fact that the majority of the antenna was realized by 3D printing, the associated system still relies on an off-the-self waveguide adapter that suffers from unavoidable mismatch due to reflections in the air-dielectric interface that can reduce the realized gain of the antenna.

In this study, a GRIN lens antenna with an embedded feed is realized for the first time. Such an arrangement represents an all-dielectric alternative with no metallic walls. Also, it demonstrates the application of a zero focal length GRIN lens. In our recent study [1], we have presented the derivation of new formulas based on Geometrical Optics for a compact GRIN lens with embedded feeder (i.e., placed at a null focal length F=0). By assuming that the focus is inside the medium, the radially varying refractive index profile is derived in analytical form via the inverse truncated Abel transform. The refractive index profile is given as a function of the lens geometrical parameters, namely the lens radius and thickness. The GRIN solution for infinite cylinder and radial graded index already existed in the literature [18], [19], named by the author in [19] "Mikaelian Lens". However, it was mostly used in the framework of fiber optics and, to the authors' knowledge, this is the first time an antenna with an embedded feed is realized.

In this work, we proceed to the practical realization, by using 3D printing technology, and to the experimental verification of the GRIN lens with an integrated feeder proposed in [1]. All the challenges related to the unavoidable discretization of the refractive index, required for the practical realization, are presented and discussed. To validate the 3D printed GRIN lens performance, the full 3D far-field radiation pattern is measured using our in-house spherical near-field facility in a wide frequency range between 12-22 GHz. This is accomplished by swapping the feeders operating in different frequency bands. It should be noted that the bandwidth of the antenna system is bounded to both the frequency response of the feeder, as well as to selected discretization of the perforated 3D printed GRIN lens towards the higher frequencies. The directivity and the gain are extracted.

The article is organized as follows. Section II presents the design methodology of the GRIN lens together with the discretization and unit cell design suitable for 3D printing. Section III shows numerical simulations of the designed GRIN lens using a discrete number of permittivity layers. In Section IV, the 3D printing of the GRIN lens is presented together with the characterization of the 3D printed filament. In Section V, the measurement results are provided and in Section VI conclusions are drawn.

II. GRIN LENS DESIGN AND DISCRETIZATION

Let us first consider a cylindrical GRIN lens with a continuous refractive index, varying with respect to the radial coordinate ρ, as depicted in Fig. 1 (a), (b). According to [1], the radially varying refractive index profile, allowing for the rays collimation, is given by the following equation (plotted in Fig. 1 (c)):

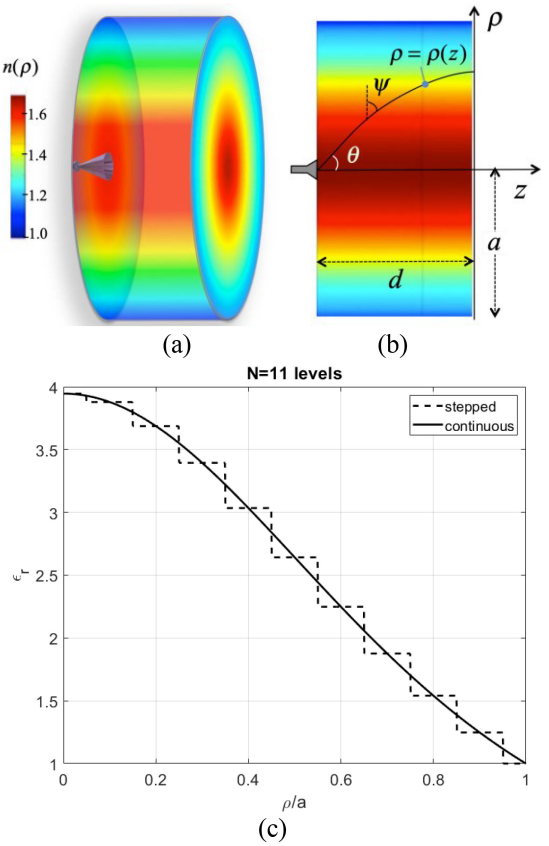

FIGURE 1. (a) 3D model and (b) 2D cut of a cylindrical zero focal length GRIN lens. The extreme ray-path passing through the lens is also shown. The refractive index distribution, reproduced from [1], is depicted by using a colored scale. (c) Continuous and staircase permittivity distribution in 11 levels.

$$n(\rho) = \frac{n_0}{\cosh\left(\frac{\pi}{2d}\rho\right)} \tag{1}$$

where the maximum refractive index as a function of the thickness-to-radius ratio d/a is given by:

$$n_0 = \cosh\left(\frac{\pi a}{2d}\right) \tag{2}$$

Here we select the thickness-to-radius ratio to be $d/a = 1.2$ and as a result the maximum refractive index is $n_0 = 2$ (or permittivity $\epsilon_r = 4$). For these lens dimensions, from [1], the calculated total aperture efficiency is 73% for a feed with $U(\theta) = cos^3(\theta)$ pattern. This is translated to an estimated directivity of 28.6 dB at 20 GHz. In order to use common thermoplastic materials for the lens fabrication such as ABS or PLA with a maximum permittivity of $\epsilon_r = 2.5 - 2.7$ respectively, the lens thickness-to-radius ratio d/a should be properly tuned in (2) to be $d/a = 1.5$.

A. CONTINUOUS AND DISCRETIZED MODEL

In this section we present the GRIN lens design together with the unavoidable discretization of the continuous permittivity distribution into a staircase distribution. Indeed, the 3D printing process requires the lens to be printed with a

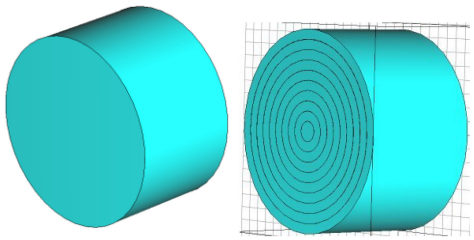

FIGURE 2. Cylindrical GRIN lens (a) continuous and (b) discretized into 11 layers.

finite number of layers of different effective permittivity. The effective permittivity required in each layer can be realized by varying the infill percentage of the dielectric material. The specific permittivity values are assigned by approximating the continuous permittivity profile given by (1) with a staircase permittivity distribution. The staircase distribution and the continuous one are plotted in Fig. 1 (c).

The discretization process produces two kinds of errors in the permittivity distribution: i) an error due to the discretization of the lens in a finite number of rings, each one with a constant permittivity ii) an error in the homogenization process due to the approximation of the constant permittivity in the *i*-th ring to a holey unit cell. Due to the selection of 11 layers, the first error is negligible.

As it is noted in [12], [13], the GRIN lens performance is affected by the number of discrete permittivity layers and the maximum unit cell (UC) size. We decide to use 11 layers for achieving a smooth transition of permittivity and to avoid phase aberrations at the lens output aperture due to fragmentation.

As a first step, we compare the effect of the discretization of the cylindrical GRIN lens via electromagnetic (EM) simulations (see Fig. 2). For this purpose, a lens with radius a=75mm (corresponding to 2.5λ at 10 GHz and 5λ at 20 GHz) and thickness *d=90mm* has been chosen. In the discretized GRIN lens (Fig. 2 (b)), each ring width is *rw=0.1 a=7.5mm*, except from the first and last which have *rw=0.05 a=3.75mm*. The different infill percentages assigned to the 3D printer, and corresponding to the different permittivity levels, are given in Table 1. The lowest permittivity for the lens is set to $\varepsilon_{r,min} = 1.5$ due to fabrication limitations. The unit cell size used in the simulations of the perforated GRIN lens prior to 3D printing is also listed in the last column of Table 1.

In order to link the required infill percentage F with the specific effective permittivity from the staircase model, a permittivity measurement is done for different infill values using a rectangular sample. More details are given in Section IV. The direct measurements of the permittivity allow to reduce the homogenization error.

From the EM simulation we derive a directivity of 29 dB at 20 GHz for the continuous model of Fig. 2a, while for the discretized model of Fig. 2b, we find a directivity of 28.8 dB, which is only 0.2 dB reduced. This result confirms the absence of phase errors due to the lens discretization.

TABLE 1. Ring width and effective permittivity using PREPERM ABS 500 as host material printed with nozzle 0.6mm, following the curve in Fig. 2.

Ring	Radius	ε_r	F Infill percentage	b unit cell size [mm]
#1 (center)	0-0.05a	4	87	0.48
#2	0.05a-0.15a	3.88	84	0.53
#3	0.15a-0.25a	3.69	80	0.63
#4	0.25a-0.35a	3.39	73	0.8
#5	0.35a-0.45a	3.03	63	1.06
#6	0.45a-0.55a	2.64	53	1.47
7	0.55a-0.65a	2.25	41	2.13
8	0.65a-0.75a	1.88	29	3.3
9	0.75a-0.85a	1.54	17	5.8
10	0.85a-0.95a	1.3	8	10
11	0.95a-1a	1	-	-

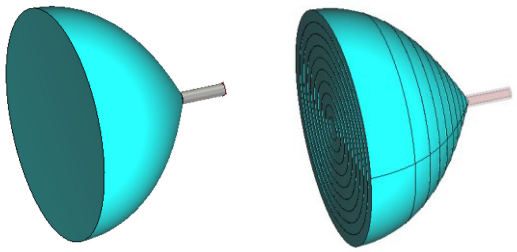

FIGURE 3. Shaped GRIN lens (a) continuous and (b) discretized into 10 layers.

A further modification of the cylindrical GRIN lens is considered as an attempt to reduce weight and volume. In [1], assuming the GO approximation, the analytical expression for the ray-trajectories inside the GRIN lens has been derived (3).

$$\rho = \frac{1}{\gamma}\sinh^{-1}(\tan\theta\,\sin(\gamma z))$$
$$\theta_{\max} = \tan^{-1}\left(\sinh\left(\frac{\pi a}{2d}\right)\right) = \tan^{-1}\left(\sqrt{n_0{}^2 - 1}\right) \quad (3)$$

With the support of an in-house code implementing a ray-tracing algorithm, we noticed that only a few rays exceed the angle θ_{max} (see Fig. 1 (b)) hence contributing to negligible spill-over. Thus, a possible improvement of the cylindrical GRIN lens with the embedded feeder is a shaped GRIN lens following the extreme ray-path ((3) for $\theta = \theta_{max}$), This opens the possibility of the realization of an all-dielectric lens-antenna (see Fig. 3).

The shaped GRIN lens in [1] ('cup lens' in the following) has negligible performance deterioration with respect to the cylindrical shape and it allows for weight and cost reduction since less material is used. Indeed, we have seen from simulations that the directivity of the continuous cup lens is 27.8 dB, −1.2 dB less than the cylindrical GRIN lens. This concept has been already discussed in [1], however has not been implemented yet. We then decide to realize the 'cup lens' instead of the cylindrical lens by using 3D printing.

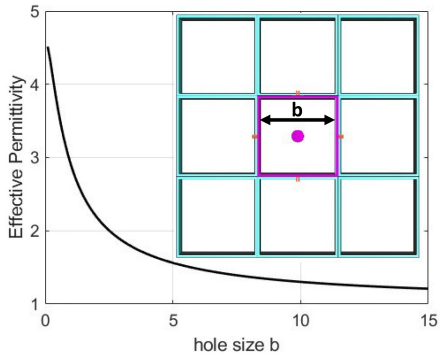

FIGURE 4. Unit cell size vs permittivity. The inset picture shows the rectangular unit cell. The thickness of the dielectric walls is fixed and it is given by the nozzle diameter 0.6mm. The measured extrusion width is measured to be 0.7mm, expanded by 20% from the nominal 0.6mm.

B. UC DESIGN

Before proceeding to the lens fabrication, we will estimate the perforated 3D printed model performance via EM simulations by modelling the same unit cell used for 3D printing. As it is shown in Fig. 4, the unit cell is a rectangular hollow dielectric cell with thickness equal to the measured extrusion width of the 3D printer. It is measured to be 0.7 mm, expanded by 20%, from the nominal nozzle diameter of 0.6mm due to heat expansion and extrusion pressure. So, in the analysis below for the unit cell we set $w = 0.7\ mm$.

The relationship between the unit cell size and the $\varepsilon_{r,eff}$ is plotted in Fig. 4. It is extracted numerically by using CST Studio Suite, using a method first used for a metamaterial unit cell in [20]. To achieve the effective permittivity gradient, the volume of the air gaps in the grid type 2D pattern in tuned in respect to the full solid host dielectric material volume. The size of the UC is $2w+b$.

To guarantee that a similar performance is achieved of the perforated model as compared to the homogeneous discretization one (satisfying the effective medium approximation), the following rules should apply at any frequency point:

- the ring width should be greater than two unit-cells [13].
- the size of the unit-cell should be at least 5 times smaller than the wavelength [16].

A smaller extrusion width w allows for a smaller unit cell size for a given infill ratio. This means that more unit cells can fit in the ring width making the effective permittivity approximation valid towards even higher frequencies and the GRIN lens bandwidth larger.

III. EM SIMULATIONS OF THE SHAPED CUP GRIN LENS

In this section, we compare the shaped GRIN lens model constructed by homogeneous layers and the model constructed by perforations. In the literature, most of the times, a discretized model of homogeneous permittivity levels is used. However, when the GRIN lens is realized via 3D printing using a single host material, this assumption of homogeneous permittivity is not yet valid. The frequency dependence of the perforated 3D printed pattern is predicted via full wave analysis. In the perforated model of the GRIN lens (Fig. 5b) each of the ten layers is filled up with a different unit cell with size d associated to the respective permittivity value, given in Table 1. In the literature, only in a few cases, such as in [21], [22], there has been an investigation via EM simulations on the performance of the fully realistic 3D printable GRIN lens model (including the perforations using the unit cell) prior to the 3D printing. This is probably because this simulation model is computationally intensive requiring high computational resources. The simulation model of the perforated cup GRIN lens is shown in Fig. 5b, realized using a single material with $\epsilon_r = 4.6$, which is the measured permittivity of the printed filament.

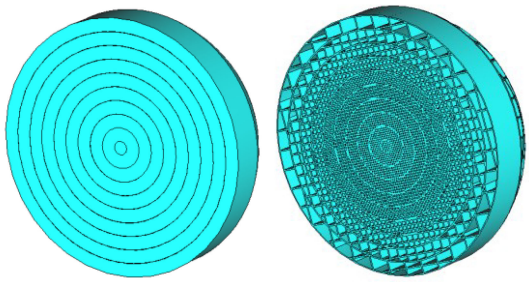

FIGURE 5. Shaped GRIN lens discretized into 10 layers of (a) homogeneous permittivity and (b) perforations according to the UC.

TABLE 2. Unit cell size versus frequency for different GRIN lens layer. The UC of Layer #1, #6 and #10 are (2w+b): 1.88mm, 2.87mm and 11.4 mm.

UC size (λ)	Layer #1	Layer #6	Layer #10
12 GHz (λ=25 mm)	λ/13	λ/9	λ/2
15 GHz (λ=20 mm)	λ/10	λ/7	λ/1.7
20 GHz (λ=15 mm)	λ/8	λ/5	λ/1.3

The effective permittivity remains valid as long as the unit-cell dimensions remain small as compared to the wavelength (effective medium approximation). As the frequency is increased, this stops to be valid and the bandwidth of the lens is limited. In Table 2, the unit cell size in terms of the wavelength is listed.

A. INTEGRATED FEED DESIGN

The integrated feed design is based on a simple circular waveguide. The selection of the waveguide as compared to other type of antennas is the easy manufacturability and the rotational symmetry, same as for the GRIN lens. The circular waveguide is loaded with the same 3d printed material with effective permittivity as the one used for the first central layer of the lens. By doing so, we avoid any unwanted reflections at the interface between the lens and the feeder. We use metallic flanges of various diameters connected with a miniaturized SSMA connector to generate the TE11 mode. In this work, two circular loaded waveguides are realized, one with ø8 and the other with ø10mm diameter, to be embedded to the shaped GRIN lens to cover the Ku (12–18 GHz)

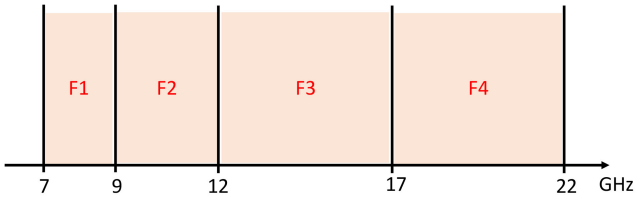

FIGURE 6. Frequency range of interchangeable circular waveguide feeds used in EM simulation.

TABLE 3. Circular waveguide feed for GRIN lenses, loaded with 3D printed material PREPERM500 with 87% infill (er=4).

Feed no.	Circular WG outer /(inner) diam.	$f_{c,TE11}$	$f_{c,TM01}$	Operating Freq. range [GHz]
F1	15 / (13) mm	6.7	8.8	7-9
F2	13 / (11) mm	8	10.4	9-12
F3	10/ (7.8) mm	11.2	14.7	12-17
F4	8 / (5.4) mm	16.3	21.2	17-22

frequency band. CST Microwave Studio simulations are carried out to design the feeding of the loaded waveguides using an SSMA connector.

To investigate the frequency response of the perforated shaped GRIN lens we used four different waveguide feeds in EM simulations (Table 3). The waveguide operating range is between the first and second cutoff mode. In [1] it had been shown that a$U(\theta) = \cos^m \theta$ pattern, with m=3 achieves the best aperture efficiency and lens illumination. All the feeds approximate this cosine pattern. Hence, they guarantee a low spillover.

In Fig. 7. the directivity of the shaped GRIN lens is plotted versus frequency, for both the discrete homogeneous and perforated models. For the homogeneous model, we observe that the trend of the directivity is increasing, meaning that there is no bandwidth limitation. As for the perforated model, we see that only at the low frequencies matches with the homogeneous model while as the frequency increases above 15 GHz, the directivity is reduced. This means that the effective medium approximation with the specific UC is no longer valid. The highest achievable directivity is spotted between 12-17 GHz at the range of 22dB.

The phase distribution at the output surface of the cup lens is derived from EM simulations. As it is observed in Fig. 6, the phase starts to be distorted at the outer rings from 15 GHz and higher.

IV. 3D PRINTING

The GRIN lens is realized using Additive manufacturing, and more specifically, Fused filament fabrication (FFF) technique. A nozzle of 0.6 mm diameter is used. The bigger nozzle diameter (standard is 0.4mm) allows for a faster printing and smaller probability of clogging, which is possible to happen in big models. The nozzle diameter determines the minimum layer thickness which should not be less than 25%. So, we selected a layer height of 0.2mm.

In the 3D printer software, or "slicer", we tune the infill percentage that describes the volume fraction of the

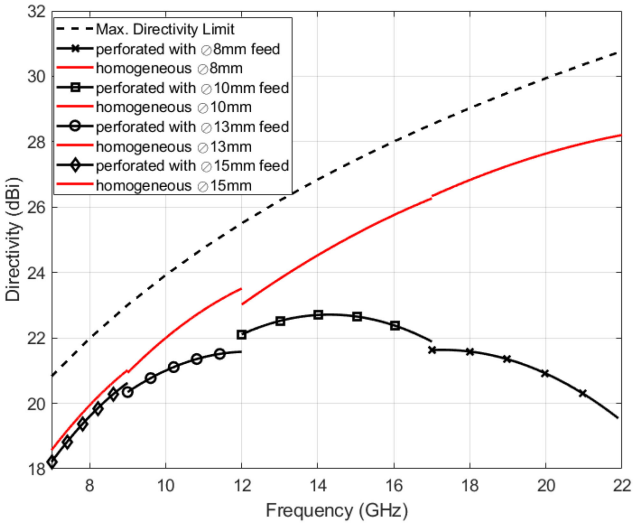

FIGURE 7. Simulated directivity of the perforated cup lens as compared to the discretized model of 10 permittivity layers.

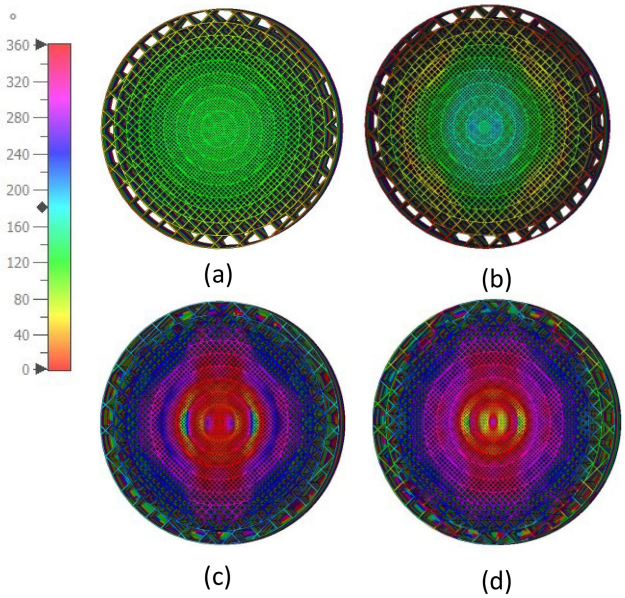

FIGURE 8. Electric field phase distribution at the shaped GRIN lens aperture for 12, 15, 18 and 20 GHz.

thermoplastic filament material to the total volume, thus the permittivity is tuned. Normally, the infill percentage is varied from 15% to 100%. As a host material, we use a custom filament PREPERM [2] based on ABS material loaded with ceramic particles to achieve a permittivity as high as 5. Due to the difficulty of reaching εr=1 using a 3D printing material, we have truncated the permittivity of the outmost ring (Ring 10) to be 1.5 instead of 1.3 that can be realized with an infill percentage of 15%.

A. PERMITTIVITY CHARACTERIZATION OF 3D PRINTED SAMPLES

The effective permittivity as a function of the infill percentage is measured using a waveguide transmission/ reflection

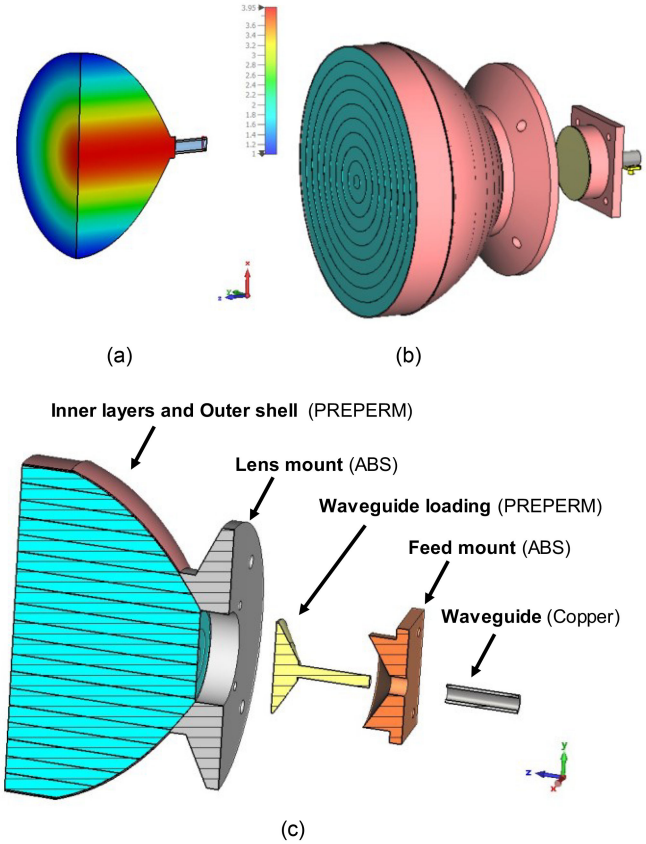

FIGURE 9. (a) 2D cross-section of the shaped GRIN lens; colour plot of the continuous permittivity distribution. (b) Finalized 3D model of the shaped GRIN lens with homogenous discrete permittivity layers. Interchangeable feeds can be used with nylon screws keeping the feed attached to the lens mount. (c) Cross-section of the exploded 3D model and the different materials used.

technique to extract the permittivity and loss tangent of 3D printed rectangular slabs. These slabs of various infill percentages are placed inside a rectangular waveguide WR159 in the range between 5-7 GHz. The S-parameters of the rectangular test samples were recorded inside the waveguide and the dielectric properties were extracted by using the Nicolson- Ross-Weir method [23], [24]. In Fig. 10a, the setup is presented and in Fig. 10b, the measured samples of effective permittivity are fitted with a polynomial model. The Wiener max model is also plotted based on the nominal permittivity of the filament, which has been used in [25] to approximate different filaments permittivity response to the filling factor. As it is observed from the measured samples in Fig. 10b, the permittivity of the full solid 3D printed sample (for material filling factor 100%), is found to be $\epsilon_r = 4.6$ in respect to the nominal permittivity of the filament $\epsilon_r = 5$. This difference is explained from the non-uniformity created by the air gaps formed between the layers and is taken into account in the lens fabrication following the permittivity model of Fig. 10b extracted from the measurements.

A second order polynomial model is used for fitting the measured samples data of the effective permittivity versus

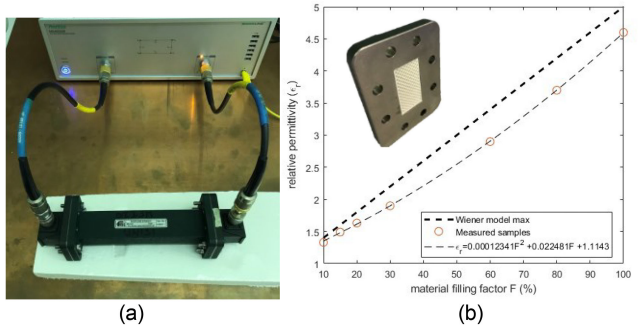

FIGURE 10. Effective permittivity as a function of the material filling factor assigned in the 3D printing. The measured data are fitted with a 2nd order polynomial function. In the inset of the figure is the waveguide flange loaded with the 3D printed dielectric, where the measured samples are measured.

TABLE 4. Settings for 3D printing of cup GRIN lens. One nozzle is used for the construction of mounting and the other for the construction of the perforated GRIN lens.

Settings	Temp nozzle °C	Temp bed °C	Speed mm/s	Layer height [mm]
PREPERM	260	110	20 infill	0.2
RAISED3D ABS	250		30	0.2

the material filling factor:

$$\epsilon_{r,eff}(F) = 1.25 \cdot 10^{-4} F^2 + 2.25 \cdot 10^{-2} F + 1.1, F \in (10, 100)$$

B. LENS FABRICATION CONSIDERATIONS

The optimization of the 3D printing parameters is an important step in the GRIN lens antenna design. In the following table (Table 4) the most important parameters together with the optimized values are listed. The fabrication of the samples and the GRIN lens prototype is done by using our in-house 3D printer (Raise 3D Pro 3) with a dual nozzle capability. The two filaments used, one for the lens mounting and one for the lens, are a standard and a custom ABS filament loaded with ceramic particles to achieve a nominal permittivity of 4 needed for the lens maximum permittivity. Using a 0.6mm nozzle, a trace width of 0.7mm was obtained and a height of 0.2mm was used to achieve good printing quality.

V. FAR-FIELD RADIATION PATTERN MEASUREMENTS

In this section, we present the far-field radiation patterns of the proposed GRIN lens antenna. The antenna measurements have been done in the spherical near-field facility of University of Siena. This part of the work is particularly important to verify the performance of the 3D printed GRIN lens in terms of the directivity and gain. The polarization of the feed is y-polarized. A standard gain horn (MVG QR2000) is used as a reference gain antenna for estimating the gain and dielectric losses of the lens antenna.

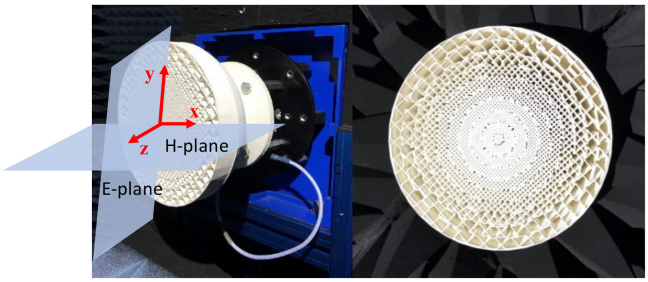

FIGURE 11. Placement in the anechoic chamber. (b) zoomed in picture of the 3D printed lens pattern.

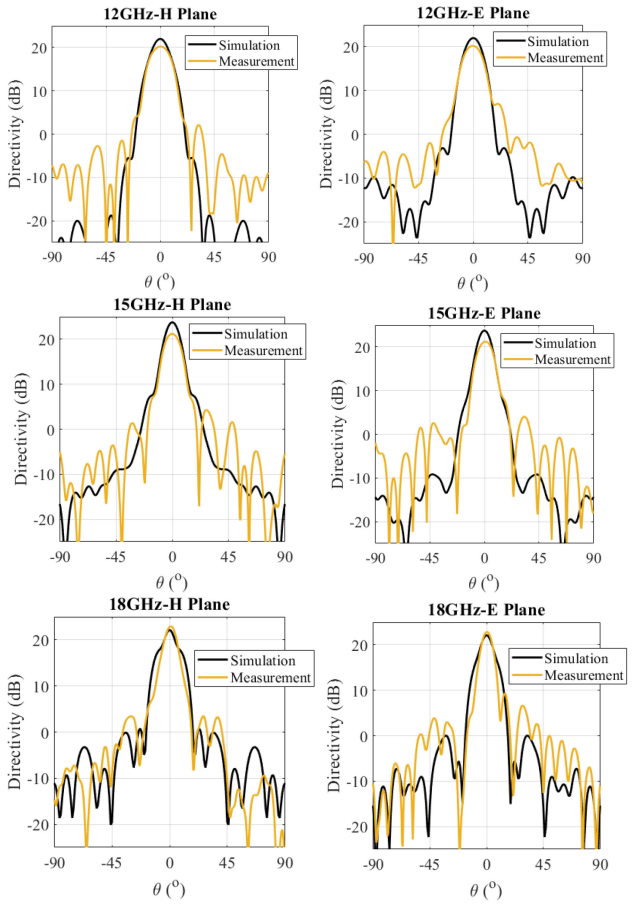

FIGURE 12. Simulated and measured radiation patterns at H- and E- plane of the shaped GRIN lens in the Ku-band for the frequencies 12, 15 and 18 GHz.

The placement of the GRIN lens antenna in the anechoic chamber is shown in Fig. 11. The E- and H-plane radiation patterns are plotted in Fig. 12. A close matching of the main beam between simulations and measurements is observed. However, the sidelobe levels (SLL) are higher in the measured patterns, especially at 12 and 15 GHz.

The measured and simulated directivity and aperture efficiency are listed in Table 5. The difference between simulation and measurement is also noted. The maximum difference is found at 12 GHz, to be 1.7 dB. The maximum measured aperture efficiency is found to be 40% at 14 GHz,

TABLE 5. Performance of the 3D printed Cup GRIN lens in terms of directivity and aperture efficiency versus frequency. The shaded rows correspond to the frequencies of the measurements.

Freq. GHz	*Feed*	*Dir. [dBi] Sim.*	*Dir. [dBi] Meas.*	*Diff. [dB]*	*Sim. Ap eff.*	*Meas. Ap eff.*
7	F1	18.2	-	-	0.55	-
8	F1	19.6	-	-	0.58	-
9	F1	20.6	-	-	0.58	-
10	F2	21	-	-	0.51	-
11	F2	21.4	-	-	0.46	-
12	F3	22	20.3	1.7	0.45	0.3
13	F3	22.4	22	0.4	0.42	0.38
14	F3	22.6	22.9	-0.3	0.38	0.40
15	F3	22.6	21.9	0.7	0.33	0.28
16	F3	22.3	21.3	1	0.27	0.21
17	F4	21.6	21.6	0	0.20	0.20
18	F4	21.6	23	-1.4	0.18	0.25
19	F4	21.3	21.5	-0.2	0.15	0.16
20	F4	20.9	21.2	-0.3	0.13	0.13
21	F4	20.3	20.4	-0.1	0.10	0.10
22	F4	19.5	18	1.5	0.08	0.05

with the directivity to be 22.9 dB. The average losses across the frequency range are found to be 2.7 dB.

Comparison with the State-of-the-art: Here we compare our findings with the current state-of-the-art in the topic of 3D printed dielectric GRIN lens antennas. In [5], a dielectric dome Lens array is 3D printed, which is used in wide angle scanning applications. Even though it is used in a different application from increasing the broadside directivity, a perforated 3D printed lens design is adopted. A similar concept to the one presented here, of the zero focal GRIN lens is presented in [28]. An H-plane horn antenna with enhanced directivity using conformal transformation optics is presented. Although, the realization is done with a parallel plate waveguide (PPW) and a fan beam pattern is provided. In Table 6, the most relevant and recent works on the activity of 3D printed GRIN lenses antennas are compared.

As compared to the reported works, our 3D printed GRIN lens appears to be more compact, low-cost and achieves an aperture efficiency of 40%. In a future work, a different UC will be designed and fabricated to increase the aperture efficiency and gain bandwidth of the proposed cup GRIN lens. To enlarge the BW of the proposed antenna even at higher frequencies, the extrusion width in the 3D printing should be reduced. The model can become even more compact when using a higher permittivity material. Finally, a multiple feeds design will be investigated for multiple beam capability.

VI. CONCLUSION

For the first time a zero focal graded index lens antenna is realized with 3D printing, allowing the feed to be embedded within the lens and not at a finite focal distance, thus making the system more compact. Different frequency bands can be covered using interchangeable feeds. A 40% measured aperture efficiency is achieved while a directivity of

TABLE 6. Comparison of different realizations of 3D printed perforated dielectric GRIN lens antennas.

Ref.	Freq [GHz]	Lens Type	Technology	Feed type	Lens Material	Diameter / Thickness (F+T)	Dir. Sim/ Meas	Ap. eff. Sim/Meas
This work	**12-22**	**Zero Focal length GRIN lens**	**3D FFF**	**Circular waveguide**	**PREPERM**	**150mm / 90mm (6λ/ 3.6λ)**	**22.6/ 22.9**	**38%/40%**
[5]	20	Dome Lens array	3D SLA	Patch array	Nylon	150 mm (10λ)	-	-
[12],[29]	34	Flat finite Focal length GRIN lens	3D FFF	Corrugated Circular OEWGs	PREPERM	88 mm / 40.5mm (10λ/4.6 λ)	26.5/ 25.7	45%/ 37%
[13]	12-40	Flat finite Focal GRIN lens	3D FFF	Rectangular OEWGs	PREPERM	120 mm /163 mm (5λ/6.5λ @ 12 GHz) or (16λ/22λ @ 40GHz)	15.1 dB @ 12 GHz/ 23.6 @ 40GHz	14%@ 12 GHz/ 9% @ 40GHz
[16]	13.4	3D shaped	3D FFF	Microstrip patch antenna	PLA	180 mm / 223.2 mm (8λ/10λ)	Sim. 26.3 dB	67%
[17]	15	Rectangular box	Material jetting (UV-cured)	Rectangular OEWGs	Verowhite	-/ 59 mm (2.95λ)	Meas 19 dB	-
[30]	27	Flat finite Focal GRIN lens	3D SLA	Microstrip patch antenna	Resin	77 mm /77mm(7λ/ 7λ)	Sim, 21.3	30%

20 dB or higher is guaranteed at the Ku-band. This study shows the challenges and performance limitations that come with 3D printing and the frequency dependence of the selected 3D printing unit cell. This work opens the possibility to simply replace traditional metallic horn antennas with this new type of all-dielectric 3D printed GRIN lens antenna.

REFERENCES

[1] F. Maggiorelli, A. Paraskevopoulos, J. C. Vardaxoglou, M. Albani, and S. Maci, "Profile inversion and closed form formulation of compact GRIN lenses," *IEEE Open J. Antennas Propag.*, vol. 2, pp. 315–325, 2021.

[2] "PREPERM^{TM}." AVIENT Website. 2023. [Online]. Available: https://www.avient.com/products/engineered-polymer-formulations/conductive-signal-radiation-shielding-formulations/preperm-low-loss-dielectric-thermoplastics

[3] D. Kalaš et al., "FFF 3D printing in electronic applications: Dielectric and thermal properties of selected polymers," *Polymers*, vol. 13, no. 212, p. 3702, 2021. [Online]. Available: https://doi.org/10.3390/polym13213702

[4] A. Goulas et al., "The impact of 3D printing process parameters on the dielectric properties of high permittivity composites," *Designs*, vol. 3, no. 4, p. 50, 2019.

[5] L. Xiao, S.-W. Qu, and S. Yang, "3-D printed dielectric dome array antenna with ±80° beam steering coverage," *IEEE Trans. Antennas Propag.*, vol. 70, no. 11, pp. 10494–10503, Nov. 2022, doi: 10.1109/TAP.2022.3195560.

[6] V. G. Ataloglou and G. V. Eleftheriades, "Synthesis of modulated dielectric metasurfaces for precise antenna beamforming," 2022, *arXiv:2211.14270*.

[7] C. Ding and K.-M. Luk, "Wideband high-gain circularly polarized antenna using artificial anisotropic polarizer," *IEEE Trans. Antennas Propag.*, vol. 67, no. 10, pp. 6645–6649, Oct. 2019, doi: 10.1109/TAP.2019.2923739.

[8] H. Yi, S.-W. Qu, K.-B. Ng, C. H. Chan, and X. Bai, "3-D printed millimeter-wave and terahertz lenses with fixed and frequency scanned beam," *IEEE Trans. Antennas Propag.*, vol. 64, no. 2, pp. 442–449, Feb. 2016.

[9] Q. Cheng et al., "Dual circularly polarized 3-D printed broadband dielectric reflectarray with a linearly polarized feed," *IEEE Trans. Antennas Propag.*, vol. 70, no. 7, pp. 5393–5403, Jul. 2022, doi: 10.1109/TAP.2022.3142735.

[10] A. A. Baba, R. M. Hashmi, M. Attygalle, K. P. Esselle, and D. Borg, "Ultrawideband beam steering at mm-Wave frequency with planar dielectric phase transformers," *IEEE Trans. Antennas Propag.*, vol. 70, no. 3, pp. 1719–1728, Mar. 2022, doi: 10.1109/TAP.2021.3111637.

[11] A. Paraskevopoulos, I. Gashi, M. Albani, and S. Maci, "Analytical formulas for refractive indices of a telescopic GRIN lens for aperture magnification," *IEEE Antennas Wireless Propag. Lett.*, vol. 21, no. 11, pp. 2206–2210, Nov. 2022, doi: 10.1109/LAWP.2022.3203914.

[12] J.-M. Poyanco, F. Pizarro, and E. Rajo-Iglesias, "3D-printed dielectric GRIN planar wideband lens antenna for 5G applications," in *Proc. 15th Eur. Conf. Antennas Propag. (EuCAP)*, 2021, pp. 1–4, doi: 10.23919/EuCAP51087.2021.9411342.

[13] S. Zhang, R. K. Arya, W. G. Whittow, D. Cadman, R. Mittra, and J. C. Vardaxoglou, "Ultra-wideband flat metamaterial GRIN lenses assisted with additive manufacturing technique," *IEEE Trans. Antennas Propag.*, vol. 69, no. 7, pp. 3788–3799, Jul. 2021, doi: 10.1109/TAP.2020.3044586.

[14] A. Paraskevopoulos, F. Maggiorelli, M. Albani, and S. Maci, "Radial GRIN lenses based on the solution of a regularized ray congruence equation," *IEEE Trans. Antennas Propag.*, vol. 70, no. 2, pp. 888–899, Feb. 2022.

[15] J. Budhu and Y. Rahmat-Samii, "3D-printed inhomogeneous dielectric lens antenna diagnostics: A tool for assessing lenses misprinted due to fabrication tolerances," *IEEE Antennas Propag. Mag.*, vol. 62, no. 4, pp. 49–61, Aug. 2020, doi: 10.1109/MAP.2019.2946566.

[16] A. Papathanasopoulos, J. Budhu, Y. Rahmat-Samii, R. E. Hodges, and D. F. Ruffatto, "3-D-printed shaped and material-optimized lenses for next-generation spaceborne wind scatterometer weather radars," *IEEE Trans. Antennas Propag.*, vol. 70, no. 5, pp. 3163–3172, May 2022, doi: 10.1109/TAP.2021.3137409.

[17] E. B. Whiting et al., "Adjoint sensitivity optimization of three-dimensional directivity-enhancing, size-reducing GRIN lenses," *IEEE Antennas Wireless Propag. Lett.*, vol. 21, no. 11, pp. 2166–2170, Nov. 2022, doi: 10.1109/LAWP.2022.3182900.

[18] E. T. Kornhauser and A. D. Yaghjian, "Modal solution of a point source in a strongly focusing medium," *Radio Sci.*, vol. 2, no. 3, pp. 299–310, Mar. 1967.

[19] L. Mikaelian, "Application of stratified medium for wave focusing," *Doklady USSR Acad. Sci.*, vol. 81, no. 4, pp. 569–571, 1951.

[20] X. Chen, T. M. Grzegorczyk, B.-I. Wu, J. Pacheco Jr., and J. A. Kong, "Robust method to retrieve the constitutive effective parameters of metamaterials," *Phys. Rev. E, Stat. Phys. Plasmas Fluids Relat. Interdiscip. Top.*, vol. 70, Jul. 2004, Art. no. 16608.

[21] M. K. T. Al-Nuaimi, W. Hong, and Y. Zhang, "Design of high-directivity compact-size conical horn lens antenna," *IEEE Antennas Wireless Propag. Lett.*, vol. 13, pp. 467–470, 2014, doi: 10.1109/LAWP.2013.2297519.

[22] H. Xin and M. Liang, "3-D-printed microwave and THz devices using polymer jetting techniques," *Proc. IEEE*, vol. 105, no. 4, pp. 737–755, Apr. 2017, doi: 10.1109/JPROC.2016.2621118.

[23] A. M. Nicolson and G. F. Ross, "Measurement of the intrinsic properties of materials by time-domain techniques," *IEEE Trans. Instrum. Meas.*, vol. 19, no. 4, pp. 377–382, Nov. 1970.

[24] J. Qi, H. Kettunen, H. Wallén, and A. Sihvola, "Different retrieval methods based on S-parameters for the permittivity of composites," in *Proc. URSI Int. Symp. Electromagn. Theory*, Berlin, Germany, 2010, pp. 588–591.

[25] A. Goulas et al., "Fused filament fabrication of functionally graded polymer composites with variable relative permittivity for microwave devices," *Mater. Design*, vol. 193, Aug. 2020, Art. no. 108871.

[26] Y. Oh, V. T. Bharambe, J. J. Adams, D. Negro, and E. MacDonald, "Design of a 3D printed gradient index lens using high permittivity ceramic," in *Proc. IEEE Int. Symp. Antennas Propag. North Amer. Radio Sci. Meeting*, Montreal, QC, Canada, 2020, pp. 1431–1432, doi: 10.1109/IEEECONF35879.2020.9330193.

[27] J. Budhu and Y. Rahmat-Samii, "A novel and systematic approach to inhomogeneous dielectric lens design based on curved ray geometrical optics and particle swarm optimization," *IEEE Trans. Antennas Propag.*, vol. 67, no. 6, pp. 3657–3669, Jun. 2019, doi: 10.1109/TAP.2019.2902737.

[28] H. Eskandari, J. L. Albadalejo-Lijarcio, O. Zetterstrom, T. Tyc, and O. Quevedo-Teruel, "H-plane horn antenna with enhanced directivity using conformal transformation optics," *Sci. Rep.*, vol. 11, Jul. 2021, Art. no. 14322.

[29] J.-M. Poyanco, F. Pizarro, and E. Rajo-Iglesias, "Cost-effective wide-band dielectric planar lens antenna for millimeter wave applications," *Sci. Rep.*, vol. 12, p. 4204, Mar. 2022.

[30] E. Garcia-Marin, D. S. Filipovic, J. L. Masa-Campos, and P. Sanchez-Olivares, "Ka-band multi-beam planar lens antenna for 5G applications," in *Proc. 14th Eur. Conf. Antennas Propag. (EuCAP)*, Copenhagen, Denmark, 2020, pp. 1–5, doi: 10.23919/EuCAP48036.2020.9135364.

Open Access funding provided by 'Università degli Studi di Siena' within the CRUI CARE Agreement